Geochimica et Cosmochimica Acta 372 (2024) 101–110

Contents lists available at ScienceDirect

Geochimica et Cosmochimica Acta

journal homepage: www.elsevier.com/locate/gca

Origin of rare earth elements in acid mine drainage traced by strontium and neodymium isotopes

Rafael León *, Francisco Macías, Carlos R. Cánovas, Ricardo Millán-Becerro, Jonatan Romero-Matos, José Miguel Nieto

Department of Earth Sciences & Research Center on Natural Resources, Health and the Environment, University of Huelva, Campus 'El Carmen', 21071 Huelva, Spain

ARTICLE INFO

Associate editor: Mélanie Davranche

Keywords:
Acid mine drainage
Strontium and neodymium isotopes
Iberian Pyrite Belt

ABSTRACT

Acid mine drainage (AMD) generated from coal and sulfide mining has attracted much interest due to the high concentrations of rare earth elements (REE) observed. However, the origin of REE in AMD and particularly the mechanism of enrichment in medium REE remain uncertain. The combined study of Sr and Nd isotopes can be used to trace the processes that control the mobility and fractionation of REE in aquatic systems such as AMD. This work reports for the first time worldwide isotopic data of Sr and Nd in AMDs from sulfide mining (Iberian Pyrite Belt, SW Spain) and compare with those in host rocks. Additionally, leaching experiments have been carried out to simulate the water–rock interactions found in these acidic systems. The results obtained strongly suggest that the origin of REE in AMDs from metal mining may be related to the preferential dissolution of shales and felsic rocks. The suitability of Sr and Nd isotopic signatures to trace the REE source in AMD-affected systems has been proven, it provides a new environmental and geochemical prospecting tool which could be useful in different geological water–rock interaction systems.

1. Introduction

Rare earth elements (REE) are a group of elements (La-Lu, Sc and Y) in critical supply risk worldwide due to a strongly monopolized market and its great demand derived from their important technological applications (Hatch, 2012; Lucas et al., 2014). The strategic search for secondary sources of REE worldwide (Binnemans et al., 2013) has encouraged in recent years numerous studies on the potential for recovery of these elements in acid mine drainage (AMD) (Ayora et al., 2016; Hedin et al., 2020; Royer-Lavallée et al., 2020; Zhang and Honaker, 2020; Arrachart et al., 2021; Larochelle et al., 2021; León et al., 2021). These acid discharges, generated during exposure of sulfides to water and oxygen primarily in areas with poor or no management practices of mining wastes (Johnson and Hallberg, 2005; Nordstrom et al., 2015), contain high amounts of metal(loid)s, and REE concentrations, several orders of magnitude higher than those of natural waters (Noack et al., 2014). Additionally, when REEs are normalized to the North American Shale Composite values (NASC) (Gromet et al., 1984), the AMDs from coal and sulfide mining areas tend to present a characteristic REE pattern, with a middle REE (MREE, Eu to Dy) enrichment with respect to light REE (LREE; La to Sm) and heavy REE (HREE; Ho to Lu) (Verplanck et al., 2001; Da silva et al., 2009; Pérez-López et al., 2010; Sahoo et al., 2012; Ayora et al., 2016). This fractionation may control the feasibility of metal recovery in AMD, considering the greater economic potential of some HREE and MREE with respect to the rest of REEs (León et al., 2021). Both mechanism that produces this enrichment, as well as the source of REE to the leachate, are still uncertain. Several hypotheses have been suggested, (1) preferential leaching of MREE-enriched phases from local lithologies (Johannesson and Zhou, 1999; Worrall and Pearson, 2001; Leybourne and Cousens, 2005; Merten et al., 2005; Sun et al., 2012; León et al., 2023), (2) mobilization of MREE by complexation of sulfur species during pyrite oxidation (Grawunder et al., 2014), (3) mineralogical control of REE by secondary precipitates (Soyol-Erdene et al., 2018), or (4) REE sorption/desorption on certain minerals, such as iron oxyhydroxides (Lozano et al., 2019a,b, 2020a,b; Liu et al., 2022). Recent studies have shown the existence of different REE-bearing mineral phases in host rocks of AMD systems, and their preferential dissolution/leaching as main mechanism of REE release during AMD formation (León et al., 2023).

The Rb/Sr and Sm/Nd isotopic systems vary due to long-term radioactive decay in the environment, and have been used as a powerful tool in petrogenetic studies and as geological tracers (Dickin, 2018).

* Corresponding author.
E-mail address: Rafael.leon@dct.uhu.es (R. León).

https://doi.org/10.1016/j.gca.2024.03.025
Received 23 May 2023; Accepted 25 March 2024
Available online 27 March 2024

The radiogenic decay of ^{87}Rb to ^{87}Sr (α-decay, $t_{1/2}$: 4.92 × 10^{10} yr) produces variations in $^{87}Sr/^{86}Sr$ ratio over time. The differences in the Sr isotopic signatures originating from the dissolution of different lithologies could be used for the characterization of water–rock interaction processes, as well as to identify the main contributors of the different components (especially alkaline earth elements) to waters in zones affected by anthropogenic pollution (Chapman et al., 2013; Wallrich et al., 2020). This issue may be addressed not directly from whole rock data, but through selective leaching or mineral separation tests (Shand et al., 2009). Thus, waters that preferentially interact with micas or clays (with high Rb content) tend to inherit high concentrations of ^{87}Sr, while waters with greater interaction with plagioclase feldspars or calcite (with relatively low Rb/Sr ratio) tend to present low concentrations of ^{87}Sr. The variation in the $^{143}Nd/^{144}Nd$ ratio is generated by the radioactive decay of ^{147}Sm to ^{143}Nd (β-decay, $t_{1/2}$: 1.06 × 10^{11} yr). Nd isotopic signatures are considered an ideal tracer for the behavior of the REEs during water–rock interactions with rocks and minerals. This is due to the similarity in atomic sizes and valence states among REEs, resulting in consistent physicochemical behavior and mobility in environmental systems. In this sense, Nd isotopes can also be used to determine the possible sources of REEs in aquatic systems such as estuarine or lake waters (Chevis et al., 2021). Therefore, these two isotopic systems could help to confirm the source of REE in AMD systems as well as other geological environments. The application of Sr-Nd isotopes in mine waters reported in literature is very limited, however, some authors have previously used Sr-Nd isotopic data (n = 8) from water and rocks from Pittsburgh coal mining area to establish the relationship of the REEs with the surrounding rocks, suggesting the preferential dissolution of MREE-rich phosphate phases as the main REE source in waters (Wallrich et al., 2020).

Compared to water–rock interactions in coal mining, those reported in sulfide mining are more intense giving rise to enhanced REE concentrations in AMD (Noack et al., 2014; León et al., 2021). In our work, novel isotopic data of Rb/Sr and Sm/Nd of rock samples and AMDs from sulfide mines of the Iberian Pyrite Belt (IPB) are analyzed, together with results of acid leaching experiments on these rocks, to confirm the origin of REE in AMD-affected systems. Therefore, our data represent a significant contribution of Nd and Sr isotopic dataset in AMD, limited to the few examples in coal mines. Selected samples in this study are representative of the lithological variety of the IPB, one of the largest metallogenic provinces of massive sulfides in the world, where the exploitation of its resources dates back to at least the last 4500 years (Nocete, 2006), with mining activity being especially intense after 1850 (Olías and Nieto, 2015). This area can be considered a natural laboratory to study the behavior of REE in AMD systems due to the high REE concentrations observed and the different chemical composition of AMD sources (León et al., 2021). The results obtained in this study may have important implications in the supply of critical raw materials worldwide, since the determination of REE-carrier mineral phases in AMD and other geological systems could help to find potential secondary deposits of these elements and their subsequent extraction.

2. Materials and methods

Rock samples (n = 35) of different lithologies (i.e., massive or disseminate sulfides, gossan, jaspers, shales, and felsic, intermediate, and mafic volcanic rocks) were collected from Poderosa and Perrunal mines. These mining areas were selected as representative zones of the IPB due to their lithological properties. Detailed geological information of both zones can be consulted in previous works (León et al., 2023). These samples, after being powdered, were subjected to acid leaching experiments (Fig. S1), simulating the interaction conditions of AMD with rocks (Wallrich et al., 2020), in order to understand the behavior and source of REE. This procedure consisted of batch sequential leaching experiments carried out under agitation with ultrapure reagents in a 40:1 liquid–solid mass ratio. First, 1 g of each rock sample was placed in contact with 1 N ammonium acetate for 4 h, releasing the easily exchangeable cations, simulating the first contact of acidic water with the surrounding rocks (Wallrich et al., 2020; Stewart et al., 2001). After washing with ultrapure water, the long-term AMD-rock interaction was simulated after leaching with 0.05 M sulfuric acid. Additionally, 27 AMD samples representative of the IPB were taken, including those outflowing from both mines under study. The location of both the rock samples and the AMD can be seen on the KMZ file - Google Earth™ included as Supporting Information.

85 samples comprising powdered rock, leachates (from leaching experiments) and AMD samples were selected for Sr and Nd isotopic analysis (Fig. S1). Isotopic analyzes were performed using a Thermo Scientific Neptune MC-ICP-MS spectrometer in the SGIker laboratories of the University of the Basque Country (UPV/EHU). Additionally, trace elements in AMDs (Table S1) were analyzed by Inductively Coupled Plasma-Mass Spectroscopy (ICP-MS) at the Research Services of the University of Huelva. Before analysis, the leachates and AMD samples were evaporated, and the resulting residue was recovered using 7 M HNO_3. On the other hand, an aliquot of the rock samples (0.05–0.2 g) was mixed with a known amount of ^{149}Sm-^{150}Nd mixed isotopic tracer (utilized for measuring Sm and Nd concentrations through isotope dilution) and the whole was dissolved using HF-HNO_3-$HClO_4$. Purification of Sr and Nd was performed by extraction chromatography on Sr-resin (Pin et al., 1994) and separation on TRU-resin and Ln-resin (Pin and Zalduegui, 1997), respectively. For the quality control of the method, blank samples, duplicate analysis, and reference standards were used. The reference materials used (NBS987 for Sr and JNdi-1 for Nd) had values in the range of our samples ($^{87}Sr/^{86}Sr$ = 0.71027 and $^{143}Nd/^{144}Nd$ = 0.512092, respectively). On the other hand, the measured blank samples presented values below the detection limit for all REEs.

$^{87}Rb/^{86}Sr$ and $^{147}Sm/^{144}Nd$ were calculated using the determined Rb, Sr, Sm and Nd concentrations. An age of 350 Ma was assumed as the average age of the different rocks of the IPB (Luz et al., 2022), and therefore initial isotopic signatures ($^{87}Sr/^{86}Sr_i$; $^{143}Nd/^{144}Nd_i$), which represents the isotopic signatures that the rock would have had at the time of its formation, were calculated using this age. $^{87}Sr/^{86}Sr_i$ was calculated from the measured ratios and the decay constant of ^{87}Rb (1.42×10^{-11} yr^{-1}), while for the calculation of $^{143}Nd/^{144}Nd_i$, the decay constant of ^{147}Sm (6.54×10^{-12} yr^{-1}) was used by applying the following equations:

$$^{143}Nd/^{144}Nd_i = ^{143}Nd/^{144}Nd - ^{147}Sm/^{144}Nd(e^{\lambda T} - 1) \quad (1)$$

$$^{87}Sr/^{86}Sr_i = ^{87}Sr/^{86}Sr - ^{87}Rb/^{86}Sr(e^{\lambda T} - 1) \quad (2)$$

Being λ the decay constants and T the age of the rocks, mentioned above.

The Nd isotopes data reported as $\varepsilon Nd_{(0,i)}$ were calculated as:

$$\varepsilon Nd_{(0,i)} = (({}^{143}Nd/{}^{144}Nd_{SAMPLE(0,i)} - {}^{143}Nd/{}^{144}Nd_{CHUR(0,i)})/{}^{143}Nd/{}^{144}Nd_{CHUR(0,i)})*10^4 \quad (3)$$

where $^{143}Nd/^{144}Nd_{\ CHUR\ (0)}$ = 0.512638 (Jacobsen and Wasserburg, 1980), and $^{143}Nd/^{144}Nd_{\ CHUR\ (i)}$ was estimated at 0.51219.

Fractionation of Sm from Nd during cortical processes involving minerals like monazite, xenotime, apatite, or garnet can cause

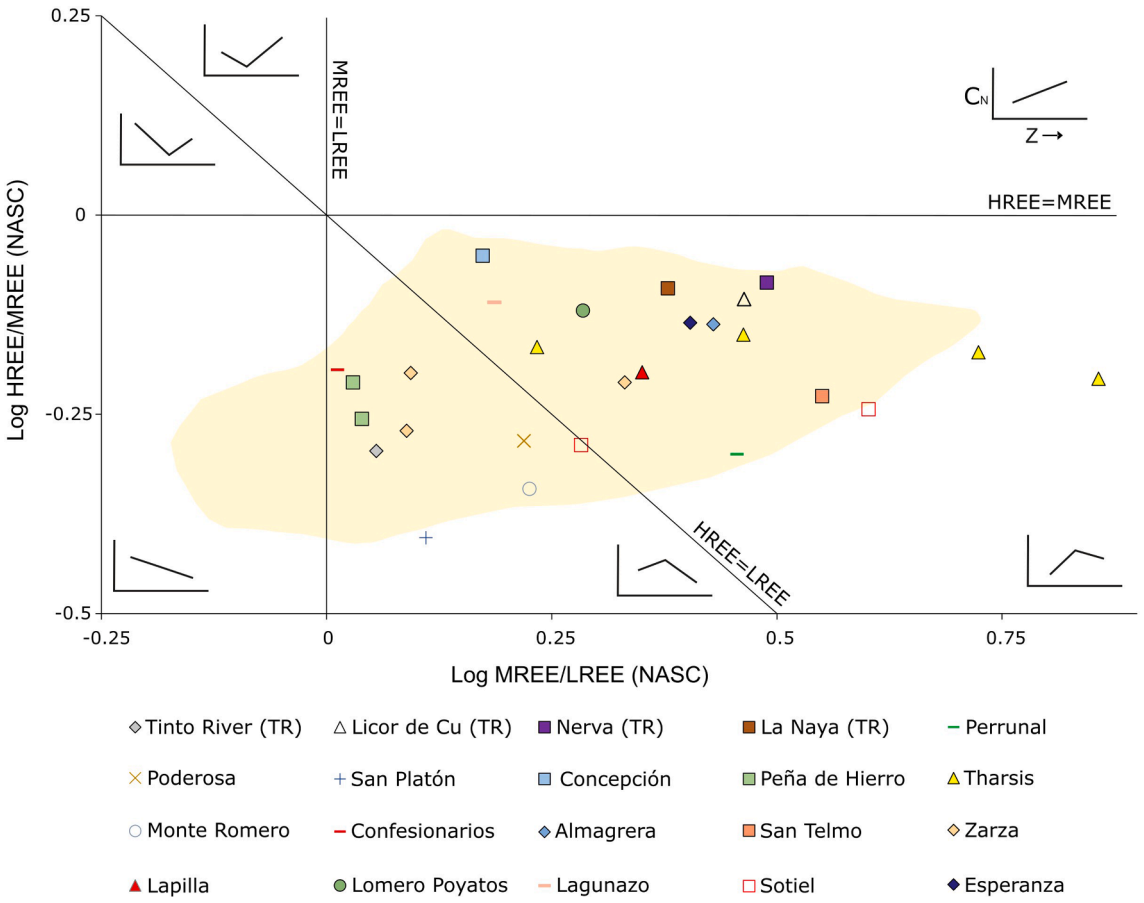

Fig. 1. Modified Stolpe diagram (Stolpe et al., 2013), showing AMD samples according to their average relative content of LREE, MREE and HREE normalized to NASC. The yellowish field represents previously reported data of AMD from the IPB (León et al., 2021).

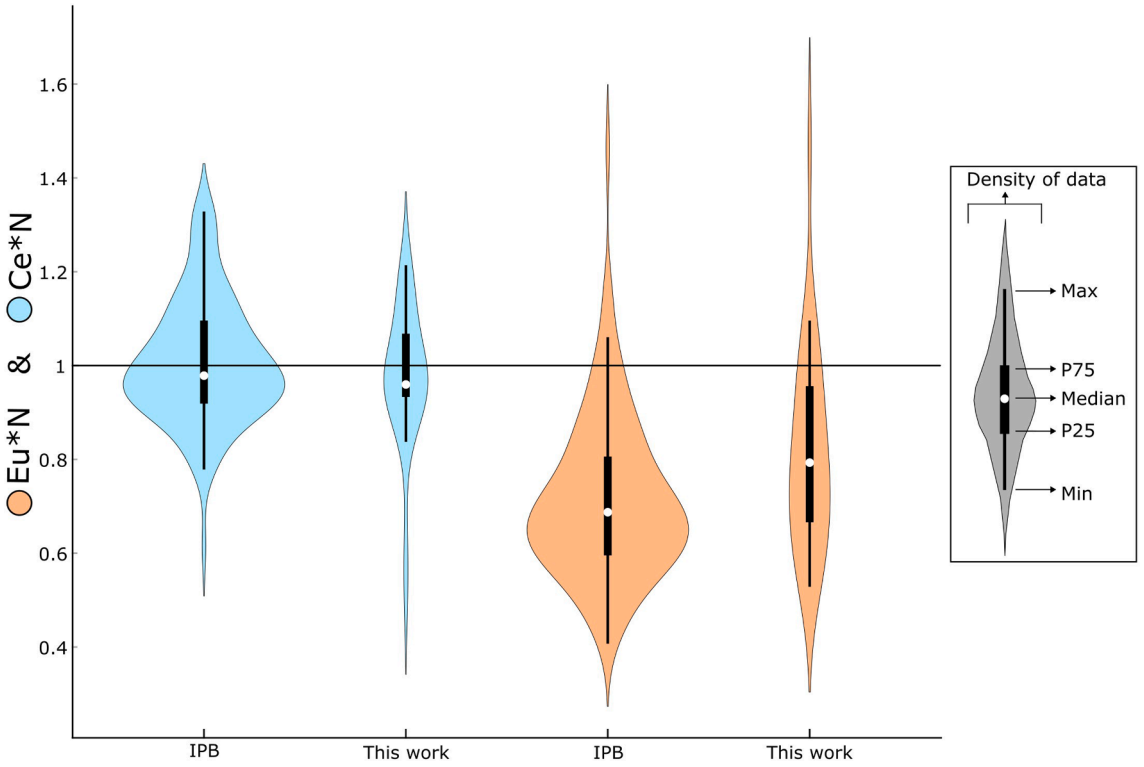

Fig. 2. Violin plot of the Eu^*_N and Ce^*_N values in the AMD previously reported in the IPB (León et al., 2021) and AMD from this work.

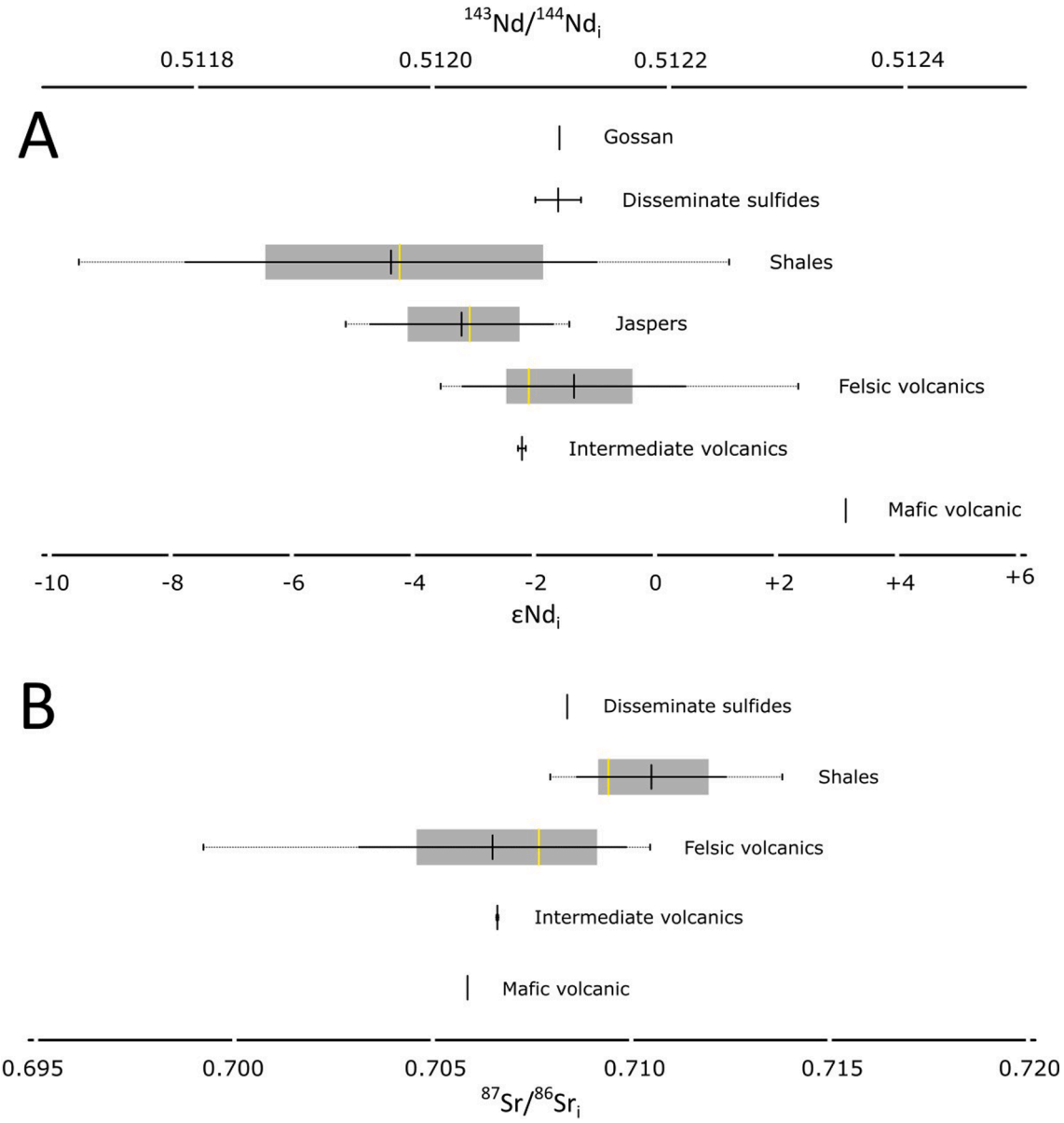

Fig. 3. Boxplot of the isotope values of Nd (A) and Sr (B) corrected to the formation age in the rock samples, depending on the lithologies.

anomalous values in the $^{147}Sm/^{144}Nd$ ratios of some samples (>0.165; Bea et al.,2023). This can lead to errors in calculating Nd-depleted Mantle (TDM) model ages. To mitigate these errors, a two-step model has been applied (Liew and Hofmann, 1988).

Finally, the Ce (Ce*N) and Eu (Eu*N) anomalies were determined by using equations (Noack et al., 2014) to interpolate the normalized values of nearby REE:

$$Ce^*_N = 2[Ce]_N / \left([La]_N + [\mathrm{Pr}]_N\right) \qquad Eu^*_N = 2[Eu]_N / \left([Sm]_N + [Gd]_N\right) \qquad (4)$$

3. Results

3.1. Geochemistry, Sr and Nd isotopes in AMD of the IPB

AMD samples taken (n = 27) exhibit a NASC-Normalized REE pattern enriched in MREE, with 17 of them having a higher relative content in HREE than in LREE with the remaining 10 showing the opposite enrichment (Fig. S2; Table S1). Fig. 1 shows the AMD samples classified based on their REE pattern normalized to NASC, according to the method of Stolpe et al. (2013), using the ratios $(MREE/LREE)_{NASC}$ and $(HREE/MREE)_{NASC}$, calculated by averaging all permutations of these inter-element ratios. The distribution of AMD samples in this graph is consistent with the variability of the REE pattern normalized to the NASC observed for AMD of the IPB in previous studies (León et al., 2021), where most of the samples showed a pattern enriched in MREE, 62 % of them with a relative enrichment in HREE with respect to LREE, while 28 % had a relative enrichment in LREE with respect to HREE. The remaining 10 % of AMDs in the IPB (León et al., 2021) shows a pattern relatively enriched in LREE and depleted in HREE with respect to MREE. Despite no sample exhibiting this latter pattern was collected in this study, there are several samples that plot on the limit between that field and the adjacent in Fig. 1.

The Ce anomaly of the samples taken in this study presents a wide variability (between 0.4 and 1.4), with most of the samples having no anomalies or slightly positive anomalies, consistent with the general trend of AMDs from the IPB (Fig. 2). This trend also appears to exist in the case of the Eu anomaly, where most samples show negative anomalies (around 0.6), with a wide range of values (between 0.3 and 1.7) (Fig. 2).

The wide geochemical variability of AMDs from the IPB is also

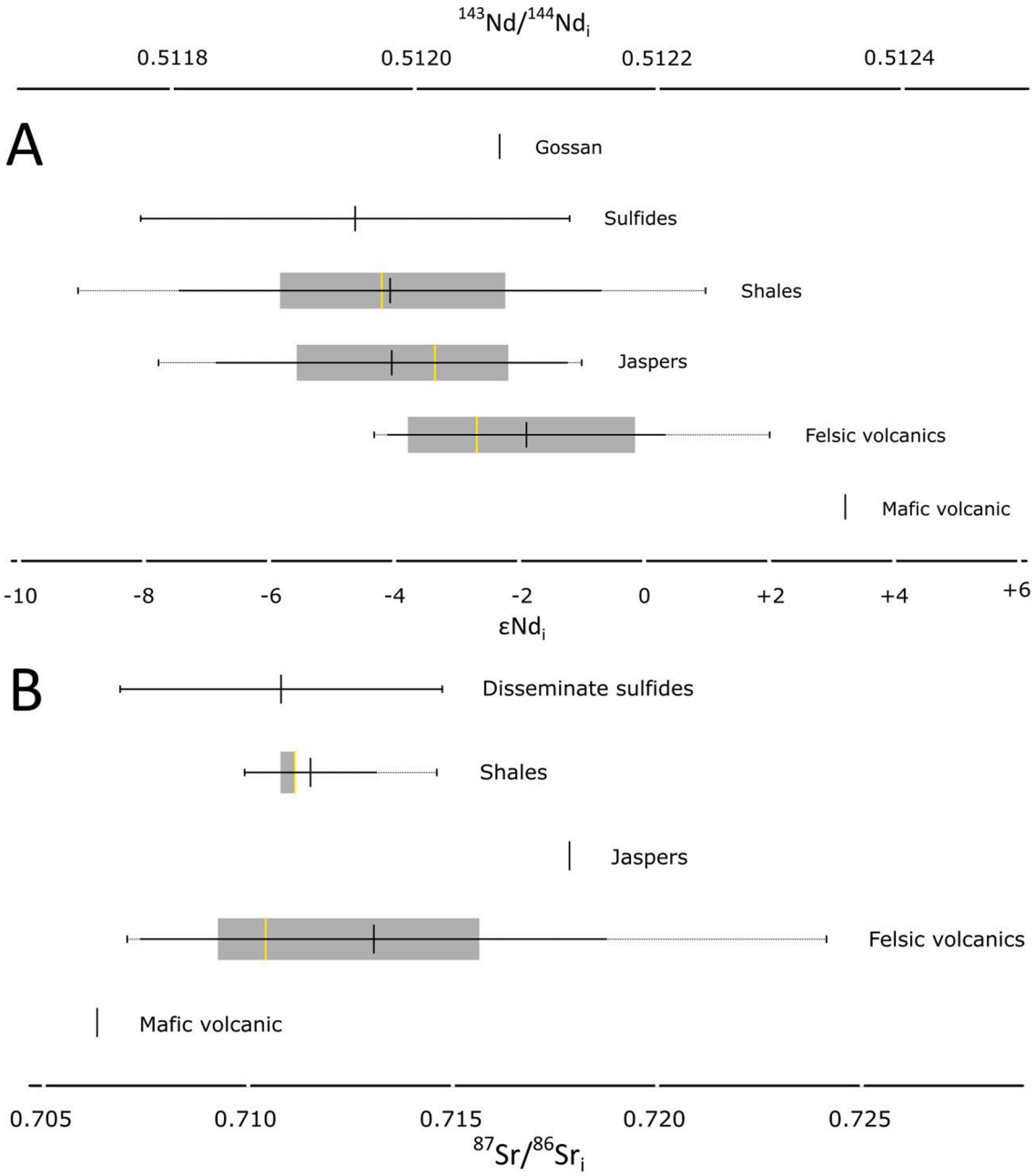

Fig. 4. Boxplot of the isotope values of Nd (A) and Sr (B) corrected to the age of formation of the rocks in the leachates samples, depending on the leached lithologies.

evidenced by the Rb/Sr and Sm/Nd isotopic data shown in Table S2. The AMD samples present variable $^{87}Sr/^{86}Sr$ isotopic ratios, with values between 0.709 and 0.720 (average of 0.714) (Table S2). These values are in agreement with those reported in AMD generated in coal mining areas, around 0.711 and 0.719 (average of 0.713) (n = 41) (Chapman et al., 2012; Wallrich et al., 2020). When the AMD data are corrected according to the formation time of the rocks with which the AMD interacts (Eq. (2), $^{87}Sr/^{86}Sr_i$ values between 0.706 and 0.717 (average of 0.712) are obtained. The Nd isotopes ($^{143}Nd/^{144}Nd_i$) in AMDs from the IPB present values between 0.5120 and 0.5126, which corresponds to negative values of εNd_0 (Eq. (3) (between −1.4 and −12.3) (Table S2). Correcting to the value of $^{143}Nd/^{144}Nd_i$ (Eq. (1), values between 0.5116 and 0.5122 are obtained, resulting in εNd_i values (Eq. (3) ranging from strongly negative (-11.9) to slightly positive (+1). These predominantly negative values (average of εNd_0 and εNd_i: −6.2 and −5, respectively) are consistent with the εNd_0 and εNd_i values reported in AMD from coal mines (average of −8.6 and −8.4 respectively) (Wallrich et al., 2020).

3.2. Sr and Nd isotopes in rocks and leaching experiments in the IPB

3.2.1. Sr and Nd isotopes in rocks

The IPB rock samples analyzed in this study present Nd isotopes ranges similar to those of AMD, with $^{143}Nd/^{144}Nd$ ratios between 0.5121 and 0.5127 (and εNd_0 between +1.9 and −13.4), and between 0.5117 and 0.5124 (εNd_i between +3.2 and −9.5) when corrected according to the mean age of the rocks (350 Ma) (Table S3). However, $^{87}Sr/^{86}Sr$ isotope data in rocks do not coincide with the AMD, with values ranging from 0.706 to 0.863. These higher values (average of 0.742) in rocks than those of AMD may be due to the existence of minerals with a high Rb content (i.e., muscovite in the shales and K-feldspar in the volcanic rocks), which may have a low solubility/kinetics of dissolution, and therefore the signature is not inherited by the AMD. The $^{87}Sr/^{86}Sr_i$ corrected values do not exactly coincide with the range of AMD either, being somewhat lower (between 0.699 and 0.713, with an average of 0.708). The hypothesis of the existence of more refractory minerals is

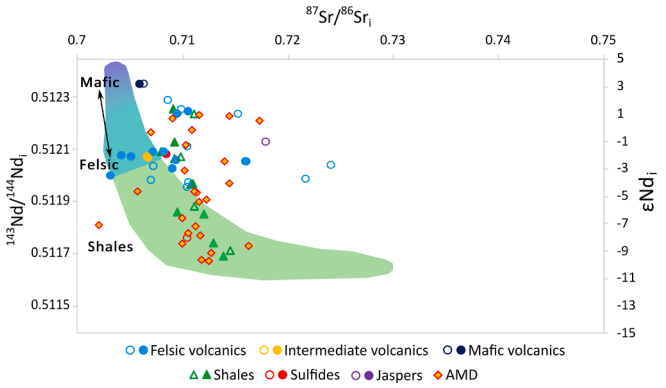

Fig. 5. $^{87}Sr/^{86}Sr_i$ versus $^{143}Nd/^{144}Nd_i$ in rock, AMD and leachate samples. The blueish and greenish fields represent the range of volcanic rocks and shales of the IPB respectively (Mitjavila et al., 1997; Valenzuela et al., 2011; Braid et al., 2012; Carvalho, 2016; Donaire et al., 2020; Pascual et al., 2021; Luz et al., 2022).

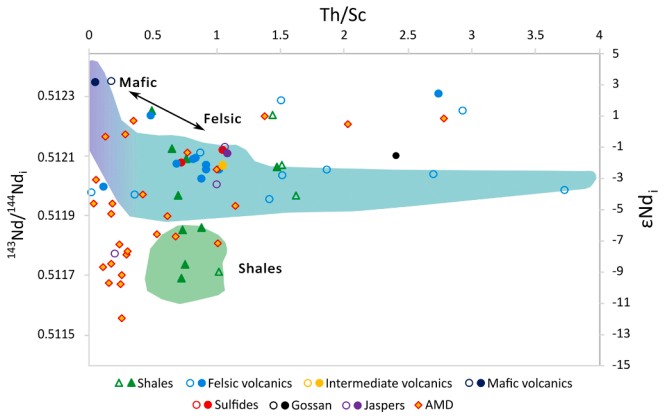

Fig. 6. Th/Sc ratio versus $^{143}Nd/^{144}Nd_i$ in rock, AMD and leachate samples. The bluish and greenish fields represent the range of volcanic rocks and shales of the IPB respectively (Mitjavila et al., 1997; Valenzuela et al., 2011; Braid et al., 2012; Carvalho, 2016; Donaire et al., 2020; Pascual et al., 2021; Luz et al., 2022).

consistent with the data obtained from the leaching experiments, which leachates show $^{87}Sr/^{86}Sr$ and $^{87}Sr/^{86}Sr_i$ ratios close to those of AMDs (average of 0.717 and 0.712, respectively) (Table S3), due to the difficulty to dissolve these reluctant minerals during the leaching experiment upon mild acidic conditions. Regarding Nd isotopes, leachates samples present similar ranges to both AMD and rock samples, with $^{143}Nd/^{144}Nd$ ratios between 0.5121 and 0.5127 (εNd_0 between + 1.9 and −9.3), while the corrected values of $^{143}Nd/^{144}Nd_i$ have the same range as those presented by rocks, between 0.5117 and 0.5124 (εNd_i between + 3.2 and −9.1).

Within the different types of rock, it can be observed that the lower $^{143}Nd/^{144}Nd_i$ values are exhibited by shales, with mean εNd_i values around −4, but with a wide range from almost +2 to −10 (Fig. 3). Higher values are showed by volcanic rocks, with values ranging from −2 and −1 for intermediate and felsic rocks, respectively, which increase to +3 in the case of mafic rocks. This trend is similar to that presented by the IPB data available in literature (Mitjavila et al., 1997; Relvas et al., 2001; Valenzuela et al., 2011; Braid et al., 2012; Carvalho, 2016; Donaire et al., 2020; Pascual et al., 2021; Luz et al., 2022) (Fig. S3) with strongly negative values in shales (mean of −8 εNd_i) and mean values of εNd_i in the volcanic rocks ranging from −3 in felsic rocks to +2 in mafic rocks. On the other hand, jaspers present slightly negative mean values of εNd_i (−3), similar to gossan (εNd_i close to −2). Sulfides presents values similar to the mean of the felsic volcanic rocks or coinciding with the range of the slates (εNd_i close to −2), since its mineralization is disseminated in these types of rocks (Fig. 3). Regarding the $^{87}Sr/^{86}Sr_i$ isotopes, most rocks have average values between 0.705 and 0.710, although felsic volcanic rocks cover a range of lower values (minimum values below 0.700) while shales can reach maximum values of 0.715. These $^{87}Sr/^{86}Sr_i$ values coincide with those reported in literature (Fig. S3), where shales have slightly high values (mean of 0.712 and maximum of 0.730) and felsic volcanic rocks have values slightly lower (minimum of 0.699). The $^{87}Sr/^{86}Sr_i$ ratios in disseminated sulfides (0.708), intermediate (0.707) and mafic volcanic rocks (0.706) are also within the IPB range (Fig. S4).

3.2.2. Sr and Nd isotopes in leaching experiments

The values of the leachate samples indicate a significant resemblance to the isotopic composition of the rocks that have been leached. In this sense, the highest εNd_i values appear in volcanic rocks, with higher values in mafic rocks ($\varepsilon Nd_i = +3.2$) and somewhat lower in felsic rocks (mean $\varepsilon Nd_i = -1.9$) (Fig. 4). The lowest values are shown by shales and jaspers, with mean εNd_i values of −4 for both samples, while the gossan sample has an intermediate value of εNd_i (−2.3). Meanwhile, the sulfide samples have a strong variation depending on its typology, that is, disseminate sulfided show εNd_i values similar to felsic rocks or some shales (−1.2), while massive sulfide exhibit strongly negative values ($\varepsilon Nd_i = -8$). In the case of the $^{87}Sr/^{86}Sr_i$ ratio, values display some variations, presenting values somewhat higher than the rocks with which they interact. In this sense, volcanic rocks show values between 0.706 during the leaching of the mafic rock sample and 0.724 for felsic rocks (Fig. 4). On the other hand, shales and sulfides present values close to 0.710, while the jasper sample have a value of 0.717.

4. Discussion

4.1. Geochemical and isotopic trends

Fig. 5 shows the trend exhibited by the volcanic rocks and shales of the IPB previously reported in literature (Mitjavila et al., 1997; Valenzuela et al., 2011; Braid et al., 2012; Carvalho, 2016; Donaire et al., 2020; Pascual et al., 2021; Luz et al., 2022). Volcanic rocks present little variation in the $^{87}Sr/^{86}Sr_i$ values (between 0.700 and 0.710), having its greatest variability in the $^{143}Nd/^{144}Nd_i$ values, with εNd_i values close to +5 in the mafic rocks and negative values in most felsic rocks ($\varepsilon Nd_i = -4$). Shales present greater variations in $^{87}Sr/^{86}Sr_i$ values (between 0.700 and 0.730) than the previous group of rocks, as well as some variation in εNd_i values (between −3 and −11).

The rocks analyzed in this study seem to follow this previously reported trend (Fig. 5A), with volcanic rocks showing mostly low values in the $^{87}Sr/^{86}Sr_i$ ratio, with high εNd_i values in mafic rock and moderate values in felsic and intermediate rocks. However, some of the felsic samples drift towards slightly higher values of the $^{87}Sr/^{86}Sr_i$ ratio. These variations could be a result of the variable levels of Rb and Sr concentrations caused by the recrystallization of carbonates and phyllosilicates, or the breakdown of feldspars, during tectonic and metamorphic processes (Luz et al., 2022). Shales present low values of εNd_i, and somewhat higher values in the $^{87}Sr/^{86}Sr_i$ ratio, but they do not seem to completely follow the trend towards values of $^{87}Sr/^{86}Sr_i$ (between 0.720 and 0.730) observed in literature. Regarding the isotopic results of both leachates and AMD samples, there seems to exist a different pattern related to rock typology. Most samples may follow the trend exhibited by shales, while another part of AMD samples present values close to the trend of the felsic volcanic rocks, but with slightly high values of $^{87}Sr/^{86}Sr_i$, as for rock samples.

The Th/Sc ratio compared to the εNd_i can be used to distinguish the origin of the rocks (i.e. volcanic or sedimentary) (Luz et al., 2019; Luz et al., 2022). As previously mentioned, volcanic rocks present the highest εNd_i values. However, a general trend can be observed when

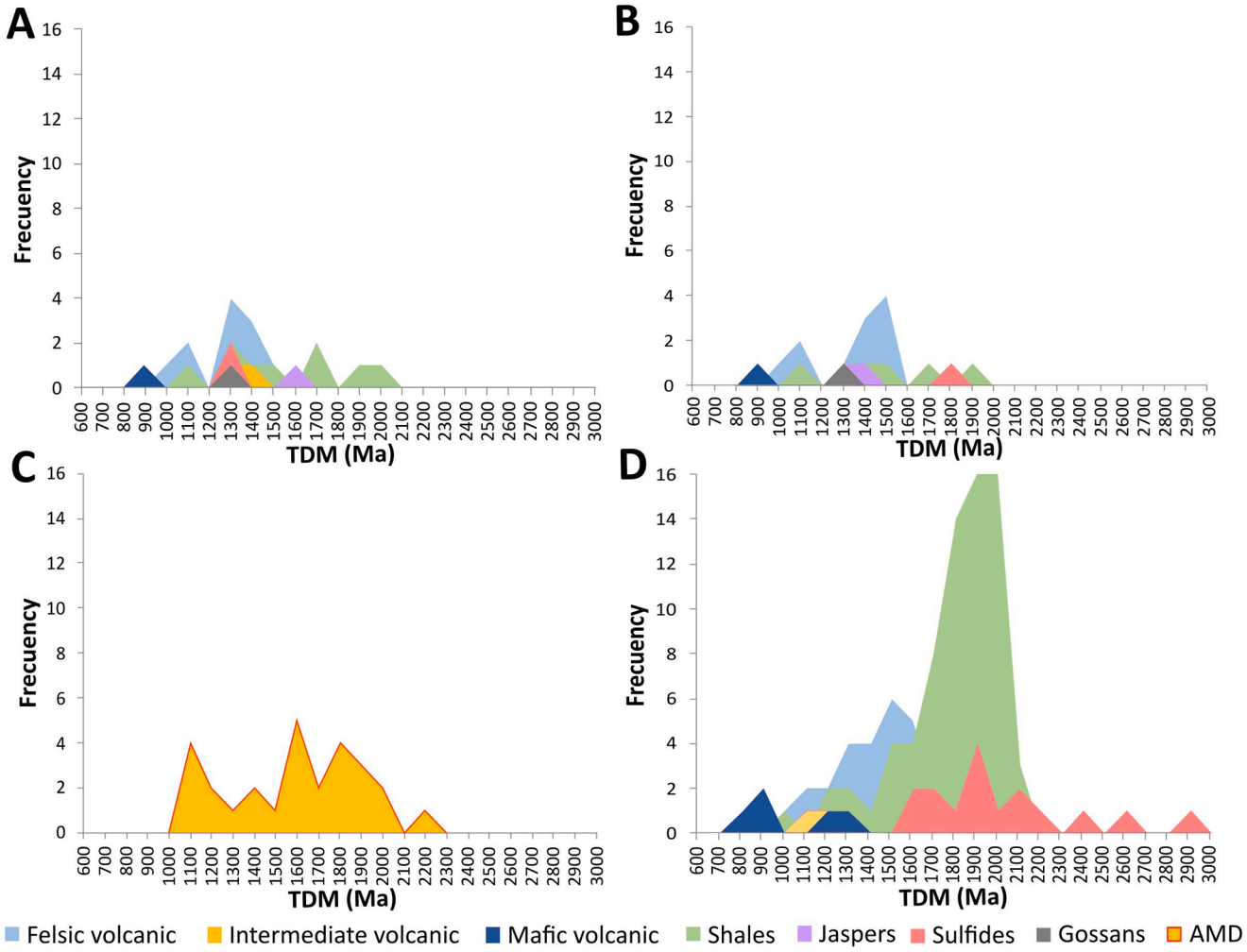

Fig. 7. Frequency plot of Nd-depleted Mantle (TDM) model ages in rock (A), leachates (B) and AMD (C) samples, and rock data available in the literature of the IPB (Mitjavila et al., 1997; Relvas et al., 2001; Valenzuela et al., 2011; Braid et al., 2012; Carvalho, 2016; Donaire et al., 2020; Pascual et al., 2021; Luz et al., 2022) (D).

compared with the Th/Sc ratio, with Th/Sc ratios close to 0 for mafic rocks and values ranging from 0.5 to 4 for felsic rocks (Fig. 6). Shales, which presented lower εNd_i values than volcanic rocks, have a defined field in the Th/Sc ratio between 0.5 and 1. Fig. 6 shows how volcanic rocks and shales in this study seem to agree with the general trend observed in rocks from the IPB. However, several shale samples align more closely with the field of the volcanic rocks of the IPB, possibly indicating the incorporation of volcanic material during deposition of the sedimentary rocks in the IPB (Luz et al., 2022). The disseminated sulfides seem to be located within the field of shales of the IPB, which is reasonable considering that sulfides are frequently hosted by these lithologies (along with volcanic rocks) and could potentially generate a geochemical imprint on them. In addition, other samples taken in this study, such as jaspers or gossan, are placed in fields close to that of volcanic rocks. Regarding the leachates resulting from these rocks (Fig. 6), leachates of volcanic rocks, shales, and jaspers follow a similar trend than the rocks. Regarding the AMD, they seem to present a certain relationship with both the rock and leachate trends (Fig. 6), with Th/Sc and εNd_i values in similar ranges (Th/Sc ratio between 0 and 3). However, a significant percentage of the samples present low Th/Sc and εNd_i values, not agreeing exactly with the rock trends of the IPB. The observed correlation among the trends of rock samples, their leachates, and AMD is noteworthy. The leachates attempt to mimic the conditions of AMD-rock interaction, and the similarity of values displayed by certain rock leachates with those of AMD suggests a relationship as a proxy for their origin. However, some leachate samples do not align with the AMD, possibly due to a shorter interaction time between water and rock during these leachates with respect to AMD generation and the presence of minerals with slower dissolution kinetics that affect these minor variations.

4.2. *Nd model ages as indicators of AMD-Rock interaction*

Another example of the relationship of the AMD and leachates with host rocks can be observed in the Nd model ages shown in Fig. 7. The rocks in this study have model ages estimated in between 800 and 2100 Ma (Fig. 7A), most of which coincide with the previous general data from the IPB (Fig. 7D) (Mitjavila et al., 1997; Relvas et al., 2001; Valenzuela et al., 2011; Braid et al., 2012; Carvalho, 2016; Donaire et al., 2020; Pascual et al., 2021; Luz et al., 2022), where mafic rocks present the most recent model ages (700–1400 Ma) and shales and sulfides the oldest (between 1000 and 2200 and 1500–3000 Ma, respectively). The felsic and intermediate volcanic rocks present intermediate model ages (between 900 and 1800 and 1000–1400 Ma, respectively). Other rock types considered in this study, without previous information in literature, such as jaspers and gossan, also exhibit intermediate model ages (between 1200 and 1700 and 1200–1400 Ma, respectively). Leachates from the rocks seem to follow a similar trend than the rocks with which they interact, with model ages ranging between 800 and 2000 Ma (Fig. 7B). Regarding the AMDs, they present model ages that vary between 1000 and 2300 Ma (Fig. 7C), with two different well-defined groups based on the data frequency. One group

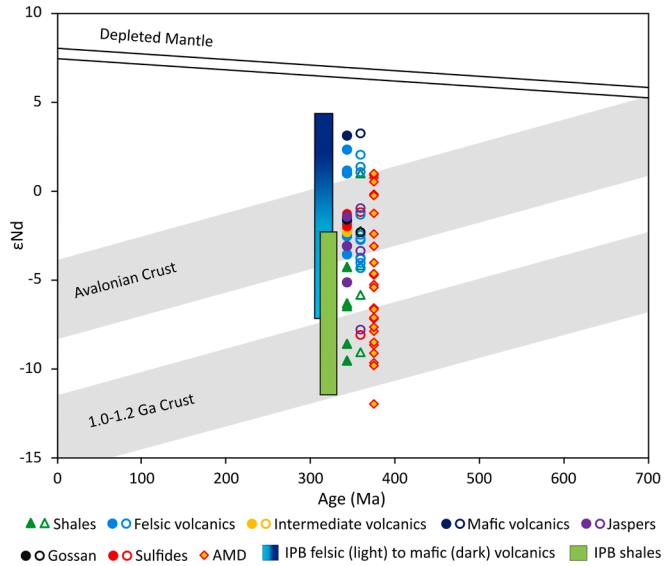

Fig. 8. εNd vs Age (Ma) diagram, showing the Nd isotope values for the rock, AMD and leachates samples compared to volcanic rocks and shales from the literature (Mitjavila et al., 1997; Valenzuela et al., 2011; Braid et al., 2012; Carvalho, 2016; Donaire et al., 2020; Pascual et al., 2021; Luz et al., 2022). Additionally, fields of evolution of the Depleted Mantle (DePaolo, 1981), Avalonian crust (Murphy et al., 1996) and 1.0–1.2 Ga crust (Samson et al., 2000) are shown.

would have model ages between 1000 and 1600 Ma, which appears to resemble the age of felsic volcanic rocks and their leachates, and a second group with model ages between 1600 and 2200 Ma, similarly to shales and their leachates. From this information it can be inferred that mafic rocks do not seem to play an important role on the AMDs composition, as they have lower model ages. On the other hand, the sulfides coincide only partially with the second group of AMDs, leaving out those sulfides with the highest model ages, which could also play a minor role in the REE release. It should be noted that although from a geochemical point of view the Nd model ages for leachates and AMD discussed above may not have genetic meaning, it does present practical interest. In this sense, in the case of AMD from the IPB, model ages lower than about 1600 Ma seem to indicate that the REEs transported in solution mainly come from a volcanic protolith, while ages greater than 1600 Ma suggest that the origin of the REEs would be from a sedimentary protolith.

4.3. Isotopic signatures and crustal evolution

Finally, Fig. 8 shows εNd values versus the age (Ma) of the rock, leachate and AMD samples, including data of local host rocks previously reported in literature. In addition, fields of evolution of the Depleted Mantle (DePaolo, 1981), the Avalonian crust of Neoproterozoic age (Murphy et al., 1996), and field of material of Mesoproterozoic age (1.0–1.2 Ga) (Samson et al., 2000) have been plotted, based on data of U-Pb detrital zircon relative probability from the South Portuguese and Pulo do Lobo zones (Braid et al., 2012; Pérez-Cáceres et al., 2017), near our study area. As previously mentioned, the εNd isotopic data of rocks in this study coincide with IPB values published in the literature. In this sense, Fig. 8 evidences how the values of volcanic rocks, especially felsic ones, fall within the evolution field of the Avalonian crust, while shales tend to be located within the evolution fields of a crust of 1.0. −1.2 Ga. In the case of other rocks such as intermediate volcanic rocks, jaspers, gossan or sulfides, they also seem to vary between both fields of evolution (with greater resemblance to the Avalonian crust). Samples obtained from leaching of these rocks seem to have a similar trend, with samples from groups that are not clearly associated with either of the two represented crusts. (Fig. 8). The leachates from felsic volcanic rocks present values close to the evolution curve of the Avalonian crust and the leachates from shales close to the crust of 1.0–1.2 Ga. The leachates from mafic volcanic rocks, like the whole rock sample, lies outside the Avalonian crust field, approaching the Depleted Mantle field. Finally, the AMD data is also consistent with the evolution trends of these two crusts, resembling the trend of both the leachates and rocks samples from the IPB, especially felsic volcanic rocks and shales, among others.

4.4. Environmental and geochemical implications

The absence of primary deposits of REE in many countries has encouraged the exploration of alternative secondary sources of these strategic metals worldwide (Binnemans et al., 2013). Among them, acid mine drainage (AMD) generated during metal mining has been identified as a promising source which could be exploited to satisfy the demand of REE due to the high concentrations commonly found in these waters (e.g., Ayora et al., 2016; León et al., 2021). However, the lack of information about the REE-carrier minerals in these geological systems makes difficult the exploration of secondary deposits suitable for exploitation. This study suggests, with the use of isotopic techniques, that the preferential dissolution of shales and felsic rocks in sulfide deposits may be the source of REE in the IPB. This information would improve the prospection efficiency for REE in these geological water–rock interaction systems, helping to identify potential sources of REE according to the abundance of shales and felsic rocks in contact with AMD waters in the different sites of the IPB and similar sulfide deposits worldwide. In addition, the application of Nd and Sr isotopes in different geological environments could provide valuable information about the origin of REE in other systems, serving as a prospection tool of REE. The identification of REE-bearing rocks and minerals in geological samples could also help to improve the metallurgical processes to extract and concentrate REE from these materials. Thus, the development of optimized metallurgical processes, supported by detailed mineralogical information, would increase the REE extraction efficiency from geological materials.

In recent years, elevated REE levels have been widely reported in different natural systems, and to date, the biological roles of REEs are still unknown, and they are now grouped as non-essential elements (Neira et al., 2022). However, if REE concentrations exceed a threshold value, they may cause severe damages to living organisms. Therefore, to determine the source of REE in different geological systems as well as their mobility could help to predict risk situations associated to REE exposure. In this sense, the application of isotopic techniques performed in this study could help to understand the potential mobility of REE in similar sulfide deposits and in other geological systems worldwide, and prevent these situations.

5. Conclusions

A Sr-Nd isotopic study has been carried out in representative rocks of the different lithologies present in the IPB (n = 29). Additionally, a large number (n = 27) of AMD representative of the geochemical variability of REE have been included in this isotopic study. In order to trace the REE sources and to analyze the influence of different lithologies on the REE composition in the AMD, acid leaching experiments have been performed on different rocks considered in this study. The isotopic signature of the studied rocks coincide with the data available in literature on rocks of the IPB. Regarding the leaching experiments carried out, leachates seem to accurately mimic the release of REE source during the AMD and host rocks interaction. This relationship can also be widely observed in isotopic evolution trends, with two distinct groups within AMD samples: a first group with model Nd ages between 1000 and 1600 Ma and with great evolution affinity to that of the Avalonian crust, composed of felsic volcanic rocks and its leachates; and a second group, with model Nd ages between 1600 and 2200 Ma, which present an

evolution more related to a 1.0–1.2 Ga crust, mainly composed of the shales from the IPB. Therefore, the isotopic signature of AMD in the IPB can be used to define the source of REE in any AMD, clearly differentiating whether the original protolith, where the REE came from, was of sedimentary or of volcanic origin. The results obtained may have important environmental and geochemical implications as provide a novel environmental and geochemical prospecting tool in different geological systems, which clarify the origin of REE in these systems and helps to identify potential secondary sources of REE worldwide.

Data availability

Data are available through Mendeley Data at https://doi.org/10.17632/yryw7t5h9m.1.

CRediT authorship contribution statement

Rafael León: Conceptualization, Data curation, Methodology, Writing – original draft, Investigation, Writing – review & editing. **Francisco Macías:** Conceptualization, Supervision, Writing – review & editing. **Carlos R. Cánovas:** Supervision, Writing – review & editing. **Ricardo Millán-Becerro:** Methodology, Writing – review & editing. **Jonatan Romero-Matos:** Methodology, Writing – review & editing. **José Miguel Nieto:** Conceptualization, Funding acquisition, Supervision, Writing – review & editing, Project administration.

Declaration of competing interest

The authors declare that they have no known competing financial interests or personal relationships that could have appeared to influence the work reported in this paper.

Acknowledgements

This research was supported by the AIHODIEL project (PYC20 RE 032 UHU) co-financed by the FEDER program in Andalucía for the period 2014–2020, LIFEWATCH-INDALO project, and ERA-MIN3 SuMRee project (PCI2024-153500), financed by MICIU/AEI/10.13039/501100011033, and by the European Union NextGenerationEU/PRTR. C.R Cánovas thanks the Spanish Ministry of Science and Innovation for the Postdoctoral Fellowship granted under application reference RYC2019–027949-I. Jonatan Romero-Matos is financed by a FPU program of the Spanish Ministry of Education of Vocational Training (FPU20/04441). Ricardo Millán-Becerro also acknowledges the Spanish Ministry of Universities for the Margarita Salas Research Grant. Funding for open access charge: Universidad de Huelva/CBUA. We would also like to thank Jeffrey G. Catalano (Editor-in-Chief), Mélanie Davranche (Associate Editor), and anonymous reviewers for the support and suggestions that significantly improved the quality of the original paper.

Appendix A. Supplementary material

The Supplementary Material comprises a PDF file that contains Tables S1–S3 and Figs. S1–S4. It provides information on the REE data obtained from the collected AMD samples (Table S1) and presents figures that show the REE data normalized to the NASC (Fig. S1). Furthermore, it includes tables with the reported isotopic data, analytical errors, and parameters calculated for the AMD samples (Table S2) and rocks and their leachates (Table S3). Moreover, the PDF includes a schematic methodology figure (Fig. S1) that visually presents the procedures performed on the rock and AMD samples, along with a description of the rock leaching method. It also include a figure (Fig. S2) with the NASC normalized REE pattern of AMD samples in this study. Additionally, two figures (S3 and S4) synthesize the Sr and Nd isotopic data collected from the literature. Supplementary material to this article can be found online at https://doi.org/10.1016/j.gca.2024.03.025.

References

Arrachart, G., Couturier, J., Dourdain, S., Levard, C., Pellet-Rostaing, S., 2021. Recovery of rare earth elements (REEs) using ionic solvents. Processes 9 (7), 1202.
Ayora, C., Macías, F., Torres, E., Lozano, A., Carrero, S., Nieto, J.M., Castillo-Michel, H., 2016. Recovery of rare earth elements and yttrium from passive-remediation systems of acid mine drainage. Environ. Sci. Technol. 50 (15), 8255–8262.
Bea, F., Montero, P., Barcos, L., Cambeses, A., Molina, J.F., Morales, I., 2023. Understanding Nd model ages of granite rocks: The effects of the 147Sm/144Nd variability during partial melting and crystallization. Lithos 436, 106940.
Binnemans, K., Jones, P.T., Blanpain, B., Van Gerven, T., Yang, Y., Walton, A., Buchert, M., 2013. Recycling of rare earths: a critical review. J. Cleaner. Prod. 51, 1–22.
Braid, J.A., Murphy, J.B., Quesada, C., Bickerton, L., Mortensen, J.K., 2012. Probing the composition of unexposed basement, South Portuguese Zone, southern Iberia: implications for the connections between the Appalachian and Variscan orogens. Can. J. Earth. Sci. 49 (4), 591–613.
Carvalho, J.R.S., 2016, Zinc metallogenesis, and indium and selenium distribution at the Neves Corvo Deposit, Iberian Pyrite Belt, Portugal: Ph.D. thesis, Lisbon, Portugal, University of Lisbon, 817 p.
Chapman, E.C., Capo, R.C., Stewart, B.W., Kirby, C.S., Hammack, R.W., Schroeder, K.T., Edenborn, H.M., 2012. Geochemical and strontium isotope characterization of produced waters from Marcellus Shale natural gas extraction. Environ. Sci. Technol. 46 (6), 3545–3553.
Chapman, E.C., Capo, R.C., Stewart, B.W., Hedin, R.S., Weaver, T.J., Edenborn, H.M., 2013. Strontium isotope quantification of siderite, brine and acid mine drainage contributions to abandoned gas well discharges in the Appalachian Plateau. Appl. Geochem. 31, 109–118.
Chevis, D.A., Mohajerin, T.J., Yang, N., Cable, J.E., Rasbury, E.T., Hemming, S.R., Burdige, D.J., Martin, J.B., White, C.D., Johannesson, K.H., 2021. Neodymium isotope geochemistry of a subterranean estuary. Front. Water. 3, 778344.
Da Silva, E.F., Bobos, I., Matos, J.X., Patinha, C., Reis, A.P., Fonseca, E.C., 2009. Mineralogy and geochemistry of trace metals and REE in volcanic massive sulfide host rocks, stream sediments, stream waters and acid mine drainage from the Lousal mine area (Iberian Pyrite Belt, Portugal). Appl. Geochem. 24 (3), 383–401.
DePaolo, D.J., 1981. Neodymium isotopes in the Colorado Front Range and crust–mantle evolution in the Proterozoic. Nature 291 (5812), 193–196.
Dickin, A.P., 2018. Radiogenic isotope geology. Cambridge University Press.
Donaire, T., Pascual, E., Saez, R., Pin, C., Hamilton, M.A., Toscano, M., 2020. Geochemical and Nd isotopic signature of felsic volcanic rocks as a proxy of volcanic-hosted massive sulphide deposits in the Iberian Pyrite Belt (SW, Spain): The Paymogo Volcano-Sedimentary Alignment. Ore Geol. Rev. 120, 103408.
Grawunder, A., Merten, D., Büchel, G., 2014. Origin of middle rare earth element enrichment in acid mine drainage-impacted areas. Environ. Sci. Pollut. Res. 21 (11), 6812–6823.
Gromet, L.P., Haskin, L.A., Korotev, R.L., Dymek, R.F., 1984. The "North American shale composite": Its compilation, major and trace element characteristics. Geochim. Cosmochim. Acta 48 (12), 2469–2482.
Hatch, G.P., 2012. Dynamics in the global market for rare earths. Elements 8 (5), 341–346.
Hedin, B.C., Hedin, R.S., Capo, R.C., Stewart, B.W., 2020. Critical metal recovery potential of Appalachian acid mine drainage treatment solids. Int. J. Coal. Geol. 231, 103610.
Jacobsen, S.B., Wasserburg, G.J., 1980. Sm-Nd isotopic evolution of chondrites. Earth Planet. Sci. Lett. 50 (1), 139–155.
Johannesson, K.H., Zhou, X., 1999. Origin of middle rare earth element enrichments in acid waters of a Canadian High Arctic lake. Geochim. Cosmochim. Acta 63 (1), 153–165.
Johnson, D.B., Hallberg, K.B., 2005. Acid mine drainage remediation options: a review. Sci. Total. Environ. 338 (1–2), 3–14.
Larochelle, T., Noble, A., Ziemkiewicz, P., Hoffman, D., Constant, J., 2021. A fundamental economic assessment of recovering rare earth elements and critical minerals from acid mine drainage using a network sourcing strategy. Minerals 11 (11), 1298.
León, R., Macías, F., Cánovas, C.R., Pérez-López, R., Ayora, C., Nieto, J.M., Olías, M., 2021. Mine waters as a secondary source of rare earth elements worldwide: The case of the Iberian Pyrite Belt. J. Geochem. Explor. 224, 106742.
León, R., Macías, F., Cánovas, C.R., Millán-Becerro, R., Pérez-López, R., Ayora, C., Nieto, J.M., 2023. Evidence of rare earth elements origin in acid mine drainage from the Iberian Pyrite Belt (SW Spain). Ore Geol Rev., 105336
Leybourne, M.I., Cousens, B.L., 2005. Rare earth elements (REE) and Nd and Sr isotopes in groundwater and suspended sediments from the Bathurst Mining Camp, New Brunswick: water-rock reactions and elemental fractionation. In: Rare Earth Elements in Groundwater Flow Systems. Springer, Dordrecht, pp. 253–293.
Liew, T.C., Hofmann, A.W., 1988. Precambrian crustal components, plutonic associations, plate environment of the Hercynian Fold Belt of central Europe: indications from a Nd and Sr isotopic study. Contrib. Mineral. Petrol. 98 (2), 129–138.
Liu, H., Guo, H., Pourret, O., Liu, M., Wang, Z., Zhang, W., Gao, B., Sun, Z., Laine, P., 2022. Geochemical signatures of rare earth elements and yttrium exploited by acid solution mining around an ion-adsorption type deposit: Role of source control and potential for recovery. Sci. Total. Environ. 804, 150241.
Lozano, A., Ayora, C., Fernández-Martínez, A., 2019a. Sorption of rare earth elements onto basaluminite: The role of sulfate and pH. Geochim. Cosmochim. Acta 258, 50–62.

Lozano, A., Fernández-Martínez, A., Ayora, C., Di-Tomamaso, D., Poulain, A., Rovezzi, M., Marini, C., 2019b. Solid and aqueous speciation of yttrium in passive remediation systems of acid mine drainage. Environ. Sci. Technol. 53, 11153–11161.
Lozano, A., Ayora, C., Macias, F., Leon, R., Gimeno, M.J., Auque, L., 2020a. Geochemical behavior of rare earth elements in acid drainages: Modeling achievements and limitations. J. Geochem. Explor. 216.
Lozano, A., Ayora, C., Fernández-Martínez, A., 2020b. Sorption of rare earth elements on schwertmannite and their mobility in acid mine drainage treatments. Appl Geochem. 113.
Lucas, J., Lucas, P., Le Mercier, T., Rollat, A., Davenport, W.G., 2014. Rare earths: science, technology, production and use. Elsevier.
Luz, F., Mateus, A., Figueiras, J., Tassinari, C.C., Ferreira, E., Gonçalves, L., 2019. Recognizing metasedimentary sequences potentially hosting concealed massive sulfide accumulations in the Iberian Pyrite Belt using geochemical fingerprints. Ore Geol. Rev. 107, 973–998.
Luz, F., Mateus, A., Ferreira, E., Tassinari, C.G., Figueiras, J., 2022. Pb-Nd-Sr Isotope Geochemistry of Metapelites from the Iberian Pyrite Belt and Its Relevance to Provenance Analysis and Mineral Exploration Surveys. Econ. Geol. 117 (2), 423–454.
Merten, D., Geletneky, J., Bergmann, H., Haferburg, G., Kothe, E., Büchel, G., 2005. Rare earth element patterns: a tool for understanding processes in remediation of acid mine drainage. Geochemistry 65, 97–114.
Mitjavila, J., Marti, J., Soriano, C., 1997. Magmatic evolution and tectonic setting of the Iberian Pyrite Belt volcanism. J. Petrol. 38 (6), 727–755.
Murphy, J.B., Keppie, J.D., Cude, M.P., Dostal, J., Waldron, J.W., 1996. Geochemical and isotopic characteristics of Early Silurian clastic sequences in Antigonish Highlands, Nova Scotia, Canada: constraints on the accretion of Avalonia in the Appalachian-Caledonlde Orogen. Can. J. Earth. Sci. 33 (3), 379–388.
Neira, P., Romero-Freire, A., Basallote, M.D., Qiu, H., Cobelo-García, A., Canovas, C.R., 2022. Review of the concentration, bioaccumulation, and effects of lanthanides in marine systems. Front. Mar. Sci. 9, 920405.
Noack, C.W., Dzombak, D.A., Karamalidis, A.K., 2014. Rare earth element distributions and trends in natural waters with a focus on groundwater. Environ. Sci. Technol. 48 (8), 4317–4326.
Nocete, F., 2006. The first specialised copper industry in the Iberian peninsula: Cabezo Juré (2900–2200 BC). Antiquity 80 (309), 646–657.
Nordstrom, D.K., Blowes, D.W., Ptacek, C.J., 2015. Hydrogeochemistry and microbiology of mine drainage: an update. Appl. Geochem. 57, 3–16.
Olías, M., Nieto, J.M., 2015. Background conditions and mining pollution throughout history in the Río Tinto (SW Spain). Environments 2 (3), 295–316.
Pascual, E., Donaire, T., Toscano, M., Macías, G., Pin, C., Hamilton, M.A., 2021. Geochemical and volcanological criteria in assessing the links between volcanism and VMS Deposits: A case on the Iberian Pyrite Belt, Spain. Minerals 11 (8), 826.
Pérez-Cáceres, I., Poyatos, D.M., Simancas, J.F., Azor, A., 2017. Testing the Avalonian affinity of the South Portuguese Zone and the Neoproterozoic evolution of SW Iberia through detrital zircon populations. Gondwana. Res. 42, 177–192.
Pérez-López, R., Delgado, J., Nieto, J.M., Márquez-García, B., 2010. Rare earth element geochemistry of sulphide weathering in the São Domingos mine area (Iberian Pyrite Belt): a proxy for fluid–rock interaction and ancient mining pollution. Chem. Geol. 276 (1–2), 29–40.
Pin, C., Zalduegui, J.S., 1997. Sequential separation of light rare-earth elements, thorium and uranium by miniaturized extraction chromatography: application to isotopic analyses of silicate rocks. Anal. Chim. Acta 339 (1–2), 79–89.
Pin, C., Briot, D., Bassin, C., Poitrasson, F., 1994. Concomitant separation of strontium and samarium-neodymium for isotopic analysis in silicate samples, based on specific extraction chromatography. Anal. Chim. Acta 298 (2), 209–217.
Relvas, J.M., Tassinari, C.C., Munhá, J., Barriga, F.J., 2001. Multiple sources for ore-forming fluids in the Neves Corvo VHMS Deposit of the Iberian Pyrite Belt (Portugal): strontium, neodymium and lead isotope evidence. Miner. Deposita 36, 416–427.
Royer-Lavallée, A., Neculita, C.M., Coudert, L., 2020. Removal and potential recovery of rare earth elements from mine water. J. Ind. Eng. Chem. 89, 47–57.
Sahoo, P.K., Tripathy, S., Equeenuddin, S.M., Panigrahi, M.K., 2012. Geochemical characteristics of coal mine discharge vis-à-vis behavior of rare earth elements at Jaintia Hills coalfield, northeastern India. J. Geochem. Explor. 112, 235–243.
Samson, S.D., Barr, S.M., White, C.E., 2000. Nd isotopic characteristics of terranes within the Avalon Zone, southern New Brunswick. Can. J. Earth. Sci. 37 (7), 1039–1052.
Shand, P., Darbyshire, D.F., Love, A.J., Edmunds, W.M., 2009. Sr isotopes in natural waters: Applications to source characterisation and water–rock interaction in contrasting landscapes. Appl. Geochem. 24 (4), 574–586.
Soyol-Erdene, T.O., Valente, T., Grande, J.A., de la Torre, M.L., 2018. Mineralogical controls on mobility of rare earth elements in acid mine drainage environments. Chemosphere 205, 317–327.
Stewart, B.W., Capo, R.C., Chadwick, O.A., 2001. Effects of rainfall on weathering rate, base cation provenance, and Sr isotope composition of Hawaiian soils. Geochim. Cosmochim. Acta 65 (7), 1087–1099.
Stolpe, B., Guo, L., Shiller, A.M., 2013. Binding and transport of rare earth elements by organic and iron-rich nanocolloids in Alaskan rivers, as revealed by field-flow fractionation and ICP-MS. Geochim. Cosmochim. Acta 106, 446–462.
Sun, H., Zhao, F., Zhang, M., Li, J., 2012. Behavior of rare earth elements in acid coal mine drainage in Shanxi Province. China. Environ. Earth Sci. 67 (1), 205–213.
Valenzuela, A., Donaire, T., Pin, C., Toscano, M., Hamilton, M.A., Pascual, E., 2011. Geochemistry and U-Pb dating of felsic volcanic rocks in the Riotinto-Nerva unit, Iberian Pyrite Belt, Spain: crustal thinning, progressive crustal melting and massive sulphide genesis. J. Geol. Soc. 168 (3), 717–732.
Verplanck, P.L., Antweiler, R.C., Nordstrom, D.K., Taylor, H.E., 2001. Standard reference water samples for rare earth element determinations. Appl. Geochem. 16 (2), 231–244.
Wallrich, I.L., Stewart, B.W., Capo, R.C., Hedin, B.C., Phan, T.T., 2020. Neodymium isotopes track sources of rare earth elements in acidic mine waters. Geochim. Cosmochim. Acta 269, 465–483.
Worrall, F., Pearson, D.G., 2001. The development of acidic groundwaters in coal-bearing strata: Part I. Rare earth element fingerprinting. Appl. Geochem. 16 (13), 1465–1480.
Zhang, W., Honaker, R., 2020. Process development for the recovery of rare earth elements and critical metals from an acid mine leachate. Miner. Eng. 153, 106382.